La mer 34: 108–130, 1996
Société franco-japonaise d'océanographie, Tokyo

A hindcast experiment in the East Sea (Sea of Japan)

Inkweon BANG*, Jei-Kook CHOI*, Lakshmi KANTHA*,
Charles HORTON**, Melody CLIFFORD**,
Moon-Sik SUK***, Kyung-Il CHANG***, Soo Yong NAM*** and Heung-Jae LIE***

Abstract: We describe here a hindcast experiment in the East Sea (Sea of Japan) for 1993, using a data-assimilative circulation model assimilating altimetric data. Climatological simulations and a synoptic run for 1993 are also described. The model reproduces many of the known circulation features in the East Sea. Altimetric data assimilation reproduces the anticyclonic eddy along the Polar Front displayed both by the tracks of the two drifter buoys deployed in the June of 1993 and TOPEX altimetric data.

1. Introduction

While there have been some numerical modeling studies (YOON, 1991 for example) in the Sea of Japan (East Sea), no nowcast/forecast attempt has been made so far. In this study, a near real-time nowcast/forecast system (CHOI *et al.*, 1996) developed for the Gulf of Mexico (GOM henceforth) is adapted for the East Sea (ES henceforth) and a hindcast of the circulation for 1993 is attempted. both the GOM and ES systems rely on the assimilation of altimetric data for nowcasts.

Although the ES and the GOM share many common features there are also many differences. The ES and the GOM are both deep semi-enclosed seas (mini-basins), and their circulations are strongly influenced by the inflow through their openings in the south. In the GOM, the inflow through the Yucatan Straits is deep because of the large sill depth (~1000m), while in the ES, the Korea (Tsushima) Strait has a shallow sill, only 200m deep at its deepest point. The Loop Current and eddies shed from it dominate the GOM circulation in the upper 1000 m. In the ES, the inflow through the Korea Strait carries 2–3 Sv into the ES, considerably smaller than the transport of 26–30 Sv by the Loop Current in the GOM, but nevertheless is responsible for most of the variability in the upper 300 m in the southern half of the ES. The variability in waters deeper than 300 m is principally due to deep convection and dense water formation in the northern parts during winter. No similar process exists in GOM waters below the Yucatan Strait sill depth.

The principal dynamical process in the GOM is that associated with the Loop Current. The Loop Current intrudes into the Gulf and eventually sheds eddies, which then propagate westward and dissipate in the western Gulf. In the ES, the Tsushima Current splits into two main branches after leaving the Korea Strait. The west branch, also called the East Korean Warm Current (EKWC henceforth), flows northward along the Korean coast and the east branch flows eastward along the Japanese coast. The EKWC separates from the coast at about 37–38°N and flows to the east. The east branch meanders and forms alternating warm and cold eddies along its path.

The ES and GOM differ considerably in their T–S characteristics (Fig. 1). In the GOM, the T–S structure is simple and its seasonal

*Department of Aerospace Engineering Sciences, University of Colorado Boulder, CO 80309–0431
**Naval Oceanographic Office, Stennis Space Center, MS 39529
***Korea Ocean Research and Development Institute P.O. Box 29, Ansan, Seoul 425–600, Korea

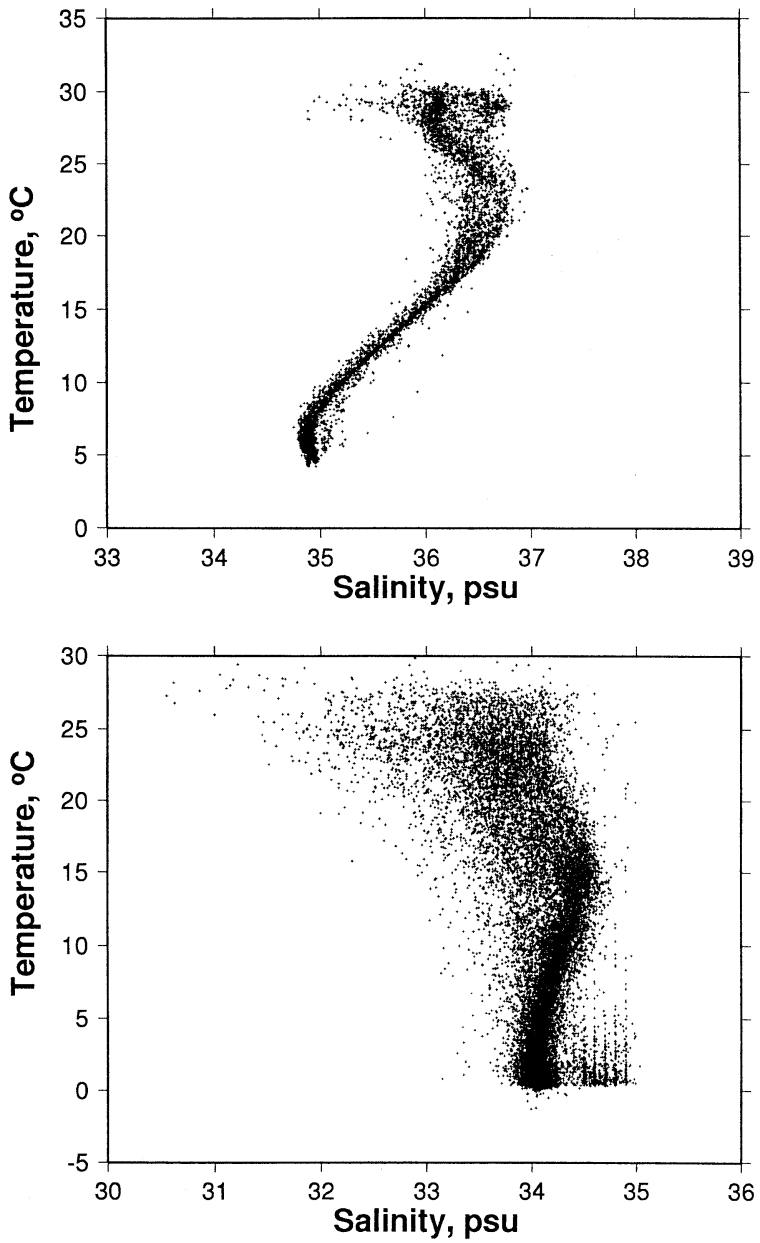

Fig. 1. T–S diagrams for the Gulf of Mexico (top) and the East (Japan) Sea (bottom) for the month of August.

variation is small. In the ES, the Polar Front running from west to east in the center of the ES separates the warm waters in the south from the colder waters in the north. The warm water in the south is due to the warm, saline Tsushima Current and shows a salinity maximum in the upper 100 m, while the cold water in the north lacks this feature. Below 400–500 m, the ES is filled with nearly homogeneous waters called the Japan (East) Sea Proper Water (ESPW). A layer of salinity minimum and dissolved oxygen maximum called Japan (East) Sea Intermediate Water (ESIW) (KIM and CHUNG, 1984) is found in the warm water

region between the Tsushima Current water and the ESPW (MORIYASU, 1972; KIM *et al.*, 1991; SENJYU and SUDO, 1993). Both the ESPW and ESIW are thought to be formed by deep convection and dense water formation processes off the Siberian coast in the north during winter.

The anticyclonic eddies in GOM elevate the sea level 50–80 cm above the surrounding, and are therefore easier to detect in altimetric data and assimilate into the model than the anticyclonic eddies in the ES (SHIN *et al.*, 1995), which rarely exceed 10 cm. Also the large spatial and temporal variability due to the meanders of the Polar Front in the ES, and the presence of numerous mesoscale features ranging in size from a few km to several tens of km, makes the nowcast/forecast task significantly more difficult than that in the GOM.

2. Methodology

The core of the nowcast/forecast system is a three-dimensional circulation model assimilating observational data using a simple optimal interpolation (OI) method. The model is a version of the sigma-coordinate model developed at Princeton (KANTHA and PIACSEK, 1993, 1996; see also BLUMBERG and MELLOR, 1987; MELLOR, 1992), and incorporates an improved turbulence closure scheme of KANTHA and CLAYSON (1994) for a better depiction of mixing processes in the upper. It incorporates a data-assimilation module (HORTON *et al.*, 1996) designed to assimilate observational data such as multi-channel sea surface temperatures (MCSST), expendable bathy-thermographs (XBT), conductivity-temperature-depth (CTD) measurements and pseudo-BTs (bathy-thermographs) from altimetry in a continuous four-dimensional assimilation mode for nowcasting purposes. In this nowcast/forecast experiment, we have assimilated only the altimetric data, as CHOI *et al.* (1996) did for the Gulf of Mexico, whereas HORTON *et al.* (1996) used MCSSTs, and XBT/CTD surveys in their application of a similar model to the Mediterranean Sea.

The model grid size is 1/5 degree in both longitude and latitude and it has 21 vertical sigma levels. The horizontal resolution is on the ragged edge of resolving large eddies, but not the whole spectrum of eddies observed in the ES. The model has three openings, Korea Strait to the south, and Tsugaru and Soya Straits to the east. Tatarskii Straits in the north connects ES to the Sea of Okhotsk but is narrow and shallow, and hence relatively unimportant to basin-wide circulation. Seasonal average values of currents (Fig. 2) from current meter measurements of INOUE *et al.* (1985, as presented in SEKINE, 1988) are used for the inflow through the Korea Strait. The total transport through the Korea Strait of a maximum of about 3.5 Sv in August and minimum of 1.6 Sv in February is prescribed (More recent ADCP observation by ISOBE *et al.* (1994) indicate a value as high as 5.6 Sv during September.). About 60% of the inflow was assigned to the Western Channel and 40% to Eastern Channel of the Korea/Tsushima Strait. This partitioning of the inflow is somewhat arbitrary, although reasonable on the average, since it surely has variability on a variety of time scales. Outflow occurs principally through the Tsugaru Straits, according to observations, although the frontal structure displayed in AVHRR suggest that the flow through the Soya Straits is not always negligible. Therefore, 80% of the outflow is assigned to the Tsugaru Strait and 20% to the Soya Strait in this study.

Temperature and salinity are prescribed as monthly average values (Fig. 2) for the inflow (SEKINE, 1988) and are advected out at outflow ports. During spring/summer, warm relatively fresh waters from the Yellow Sea (due to large river discharges there) flow into the ES and a strong stratification develops, whereas in winter, the flow is more saline and almost vertically homogeneous.

The model was initialized with annual mean temperature and salinity fields from LEVITUS (1981). The heat and salt flux boundary conditions at the surface are provided by simpel Newtonian damping to the updated monthly mean temperature and salinity of LEVITUS (updated in 1994), with a 30-day damping time scale.

Several simulations were carried out using different wind forcing. First, the model was run

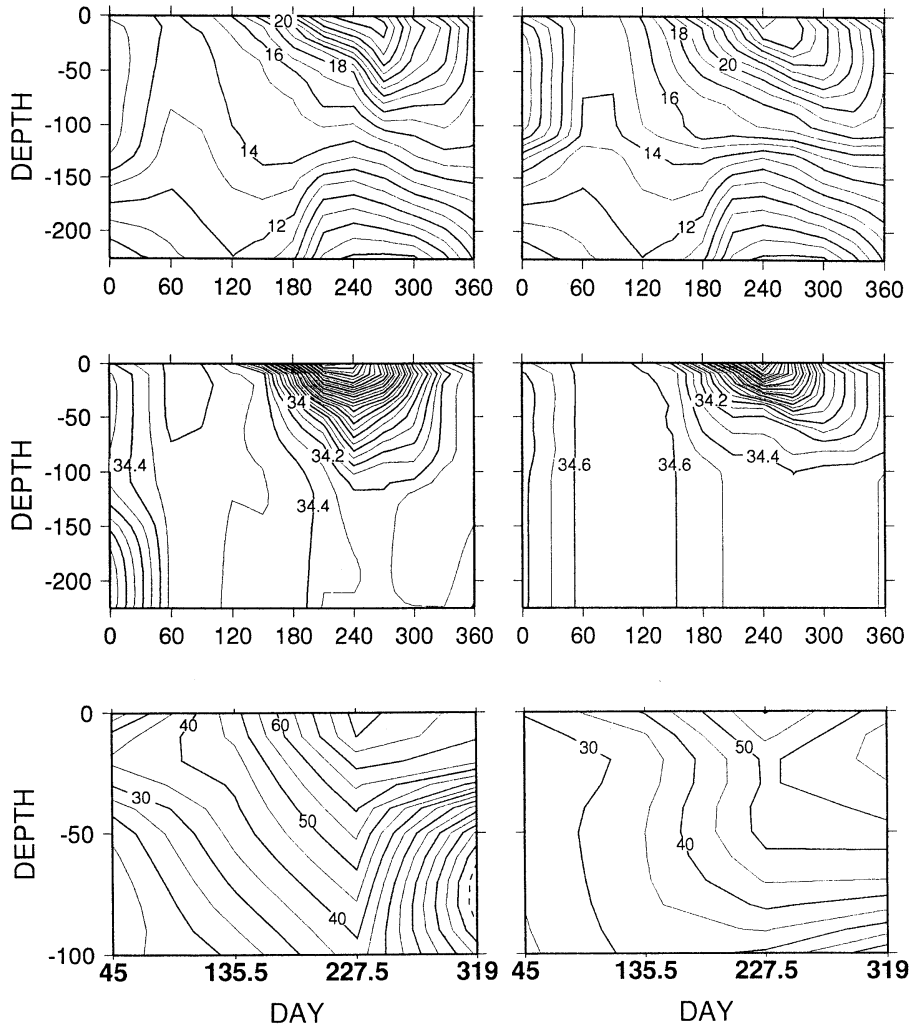

Fig. 2. Time variations of inflow temperature (top), salinity (middle) and velocity (bottom) at the western (left) and eastern (right) Channels of the Korea Strait, based on observations in Sekine (1988).

in a climatological mode forced by monthly mean HELLERMAN and ROSENSTEIN (1983) wind stress climatology. A synoptic simulation was then made for 1993 using six-hourly winds from Fleet Numerical Meteorology and Oceanography Center (FNMOC) starting from the end of the climatological run. Finally, an assimilation run was made assimilating observations from the Ocean Topography Expenriment (TOPEX) altimeter for 1993 into the model, but with the same FNMOC wind as the synoptic run. Comparison of the synoptic run and assimilation run enables us to identify the impact of assimilation. Since the assimilation technique is explained in detail in CHOI *et al* (1996), it will be discussed only briefly here.

Historical hydrographic data was passed through rigorous quality control and then subjected to Empirical Orthogonal Function (EOF) analysis to find the six most significant vertical modes of variability for each month. The dynamic height anomaly is then derived for each EOF mode, also from hydrographic data, to yield a relationship between sea

surface height (SSH) anomaly and the anomaly of the vertical temperature structure (Fig. 3). This enables SSH anomalies from altimetry to be converted to pseudo-BTs for assimilation into the dynamical model. The hydrographic data used in this study comes from the various archives : National Oceanographic Date Center, U. S. (NODC), Japan Oceanographic Data Center (JODC), Korean Oceanographic Data Center (KODC), and U. S. Navy Master Oceanographic Observation Data Set (MOODS).

Standard ionospheric, wet and dry tropospheric, Electro Magnetic (EM) bias, tidal and inverse barometric corrections on the TOPEX Geophysical Data Records (GDR) were used. In addition, a standard tilt and bias technique was used to correct for orbit errors, although for TOPEX, this procedure may not be necessary. Along-track values were averaged over 1993 and subtracted out to derive SSH anomalies from the 1993, which were then assimilated into the model track-by-track in a continuous assimilation mode, after conversion into a pseudo-BT anomalies as described above.

The temperature anomaly is assimilated into the model using the following formula :

$$T_{asm} = T_{mod} + \alpha \times [(T_{ref} + T_{anom}) - T_{mod}]$$

where α is weighting factor for observation ranging from 0 to 1. T_{ref} is taken from monthly temperature of the run without assimilation. T_{anom} is temperature anomaly derived from SSH anomaly, T_{mod} is model-computed temperature, and T_{asm} is the temperature which will be used in the next timestep instead of T_{mod}. If this factor is 1, it results in direct insertion and the model temperature (T_{mod}) is merely replaced by ($T_{ref} + T_{anom}$).

Assimilation was performed only at grid points with a water column depth of 400m or more, and data assimilation is track-by-track and continuous in time (four-dimensional assimilation). New satellite tracks are inserted at 6-hour intervals to update the sea level anomaly field. Assimilation is performed only at the first 4 timesteps (1.5 hours) of the 6-hour period. How strongly the temperature anomalies are assimilated into the model is determined by weighting factor and how long the assimilation process takes place is determined by the data insertion period. In this study, we held the insertion period fixed and varied only the weighting factors.

3. Results

3.1 Climatological Simulation

The model was run in a climatological mode for 1350 days. Fig. 4 shows that the sea level reaches an equilibrium state in the third year, and the same pattern of seasonal cycle with almost the same strength is repeated in the fourth year indicating that the barotropic spin-up process is nearly complete. To look at the baroclinic response in the upper few hundred meters where most of the seasonal fluctuation takes place, we computed the mean kinetic energy in the upper 400m (Fig. 3). The result shows that the mean kinetic energy does not increase as rapidly from the 3rd to 4th year as it has from 1st to 2nd to 3rd year. From this we may assume that the upper 400m has also reached a near-equlibrium state.

The climatological simulation reproduces the characteristic circulation features of the East Sea reasonably well (Fig. 5). The ES circulation consists of two well-developed gyres; a cyclonic gyre in the northern half and an anticyclonic in the southern half. These two gyres are separated by a Polar Front running west to east at about 40° N. In the southern anticyclonic gyre, a western boundary current, known as the East Korea Warm Current (EKWC) develops along the Korean Coast. The main source of the EKWC is the Tsushima Current through the Korea Strait. Another current (called Japan Warm Current, JWC, here) also branches off from the Tsushima Current and flows along the Japanese Coast all the way to Tsugaru Strait, the main outflow port of the ES. This branch shows strong seasonal fluctuation as a direct response to the seasonal variation in the inflow through the Korea Strait. It almost disappears during the winter-spring seasons but undergoes meandering motions during summer-fall and develops alternating small cyclonic-anticyclonic eddy stucture along its path, a characteristic clearly discernible in IR images. Part of the JWC continues northward to the Soya Straits and is responsible for the thermal fronts often observed in the

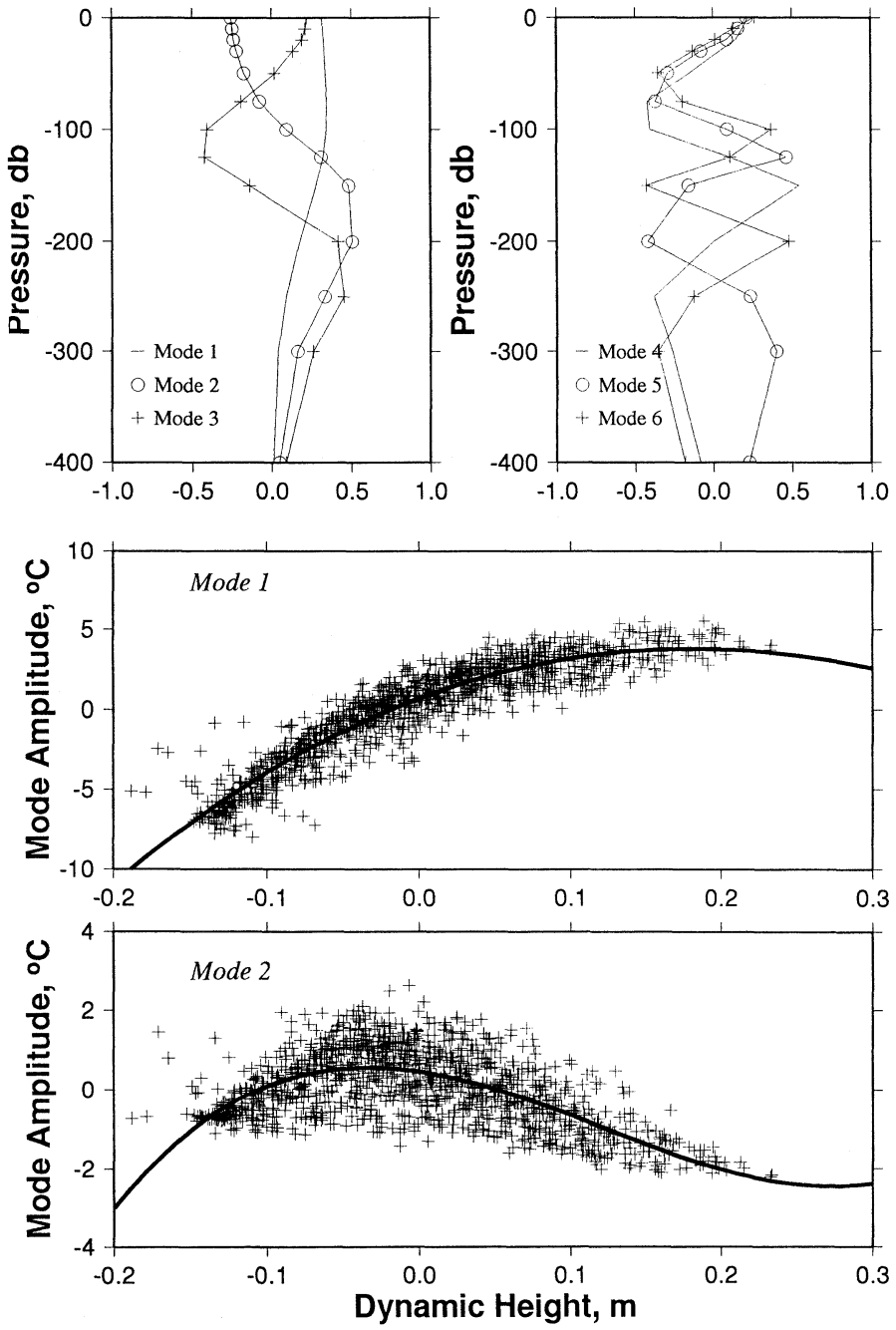

Fig. 3. Vertical profiles of the first six EOF modes of temperature variability (top) and the variation of mode amplitude with dynamic height for the first two eigen modes (middle and bottom) for the month of August.

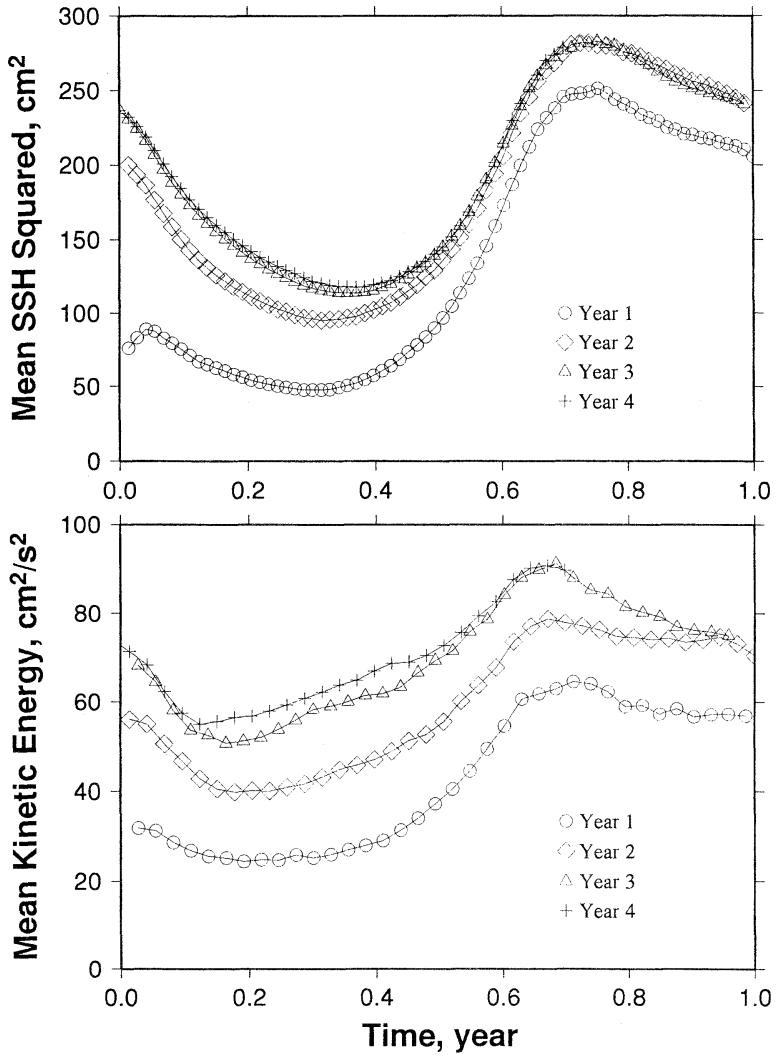

Fig. 4. Time variation of mean sea level squared (upper) and of mean kinetic energy of the upper 400 m (lower) for the climatological run.

vicinity and north of the Tsugaru Straits.

The northern gyre does not display a strong current such as the EKWC but it shows a southward-flowing current along the Russian Coast which can be identified as the Liman Current. However, the North Korean Cold Current (NKCC), which is usually observed south of the Liman Current along the Korean Coast, is not seen in these simulations, possibly because of the excessive northward intrusion of the EKWC.

One interesting and conspicuous feature in the southern anticyclonic gyre is the existence of an anticyclonic eddy near Korean Coast with its center at 131° E, 37° N. On the other hand, there are no significant mesoscale features in the central and eastern parts of the southern gyre. The model anticyclonic eddy persists almost throughout the year except the fall, and it may be identified as the Ullung Warm Eddy (hereafter UWE) observed by many researchers (ISODA and SAITOH, 1993; KIM, 1993; SHIN *et al.*, 1995).

The time-longitude plot of sea level along 37° N can be used to find out the seasonal change of the EKWC and the UWE (Fig. 6).

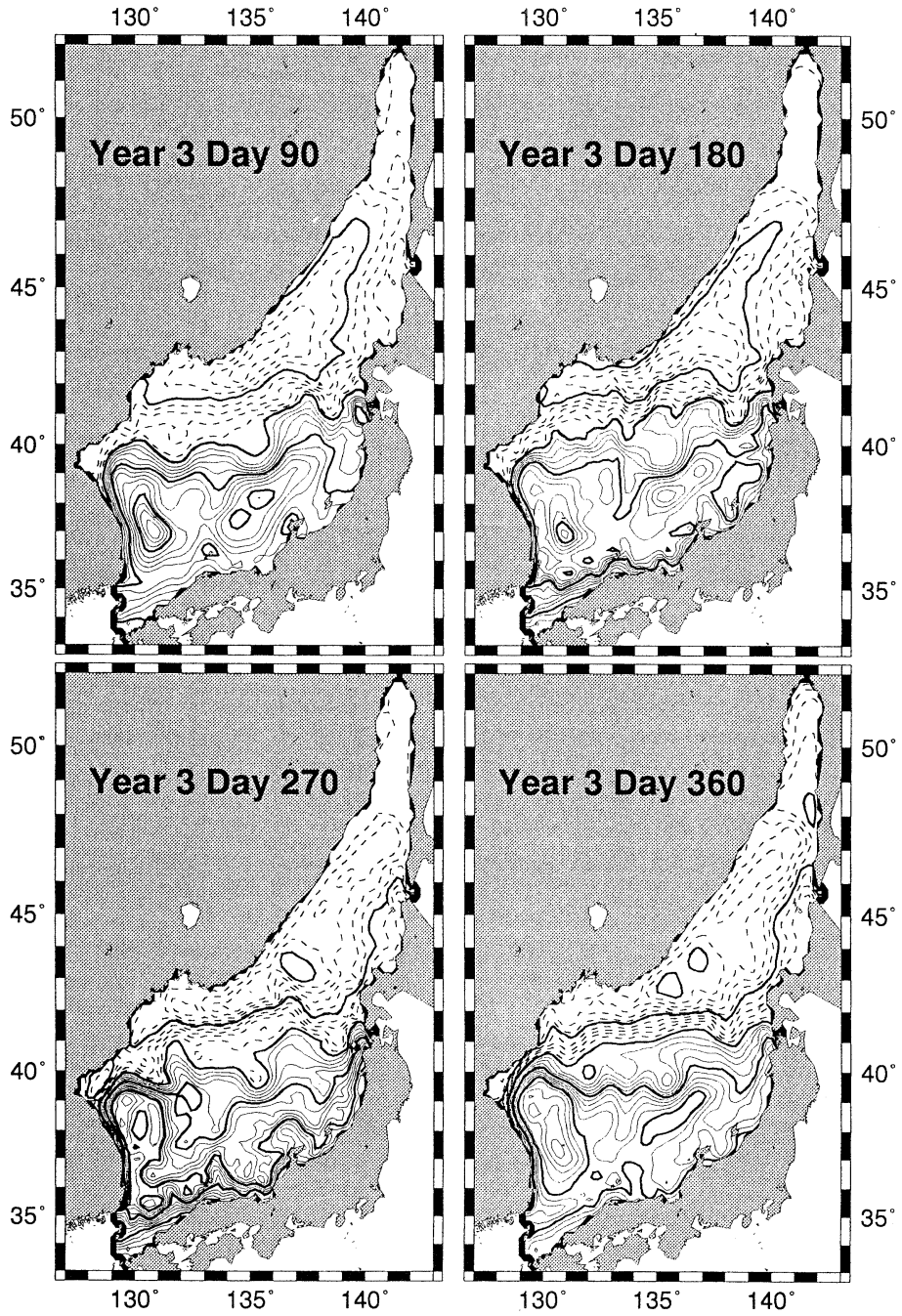

Fig. 5. Seasonal variation of sea level distribution in the climatological run. Contour interval is 2cm and the negative contours are dashed; thick lines indicate contours at 10cm intervals.

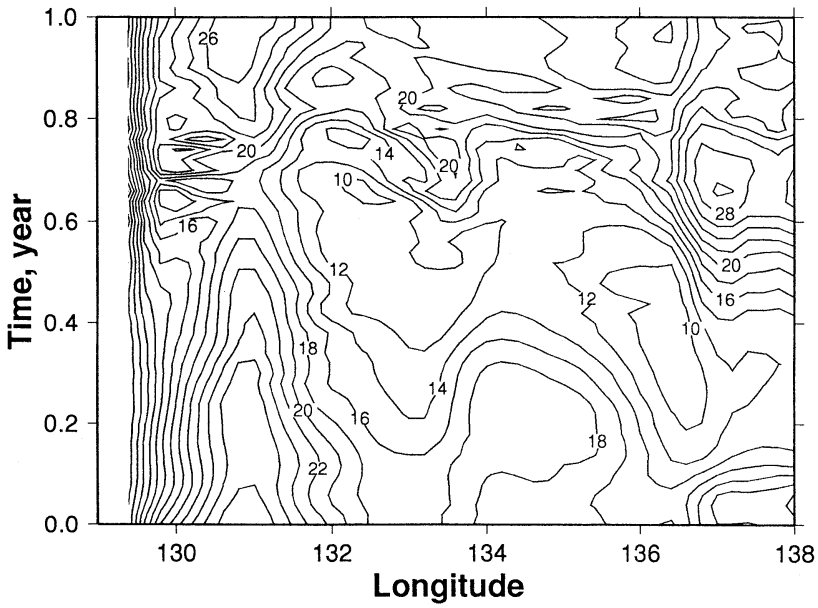

Fig. 6. Time-longitude plot of sea level (in cm) along 37°N in the climatological run.

During the first half of the year, the sea level increases gradually from Korean coast to the east and reaches its maximum at the center of the UWE. During the second half, however, the sea level increases rapidly to the east within about 50 km only from the coast. The UWE disappears during day 230–270 and small scale features appear near the EKWC. The disappearance of the UWE coincides with the time of the compression of the isolines near the coast. However, vertical section plot of v-component along 37°N (Fig. 7) shows that the EKWC stays near the coast west of 130°E all year long as a narrow current. The UWE centered about 131°E shows a northward flow in the west and a southward flow in the east. This flow pattern persists all year long except for the appearance of southward flow between EKWC and the northward flow in the west of UWE center almost the same period of the absence of UWE in the sea level signal (Fig. 6). The isotherms at depths deeper than 200m are depressed around 131°E (Fig. 8), leading to a high in the SSH at the center of the eddy. However, beginning at day 150, the isotherms in the upper 200m bulge upwards while those in deeper layers remain depressed. Therefore, the upper 200 m and the deeper layers more or less cancel each other leading to the leveling off of the sea level and "disappearance" of the UWE in the SSH fields. This pattern persists through day 270 and the isotherms in the upper 200m again becomes level at day 300.

It is interesting to note that the bulging of the isotherms beginning from day 150 leads to the formation of the relatively homogeneous water with temperature of 6–8℃ over a depth of 50 to 300m. In August, beginning at day 210, a southward current develops in the upper 100 m just offshore of the EKWC, and the UWE becomes weak and eventually disappears in the sea level signal. Day 150 corresponds to the time when the temperature in the Korea Strait becomes high at the surface, and the salinity becomes low. Day 210 is just before the transport through the Korea Strait reaches its annual maximum and the surface temperature and salinity reaches their maximum and minimum, respectively. The EKWC is also strong that the core velocity exceeds 70cm/s during day 210–270. Therefore, the inflow condition should be directly responsible for the seasonal change in the EKWC and UWE although the precise mechanism is not clear.

The model EKWC separates from the Korean Coast at a latitude of 38–39°N, at more

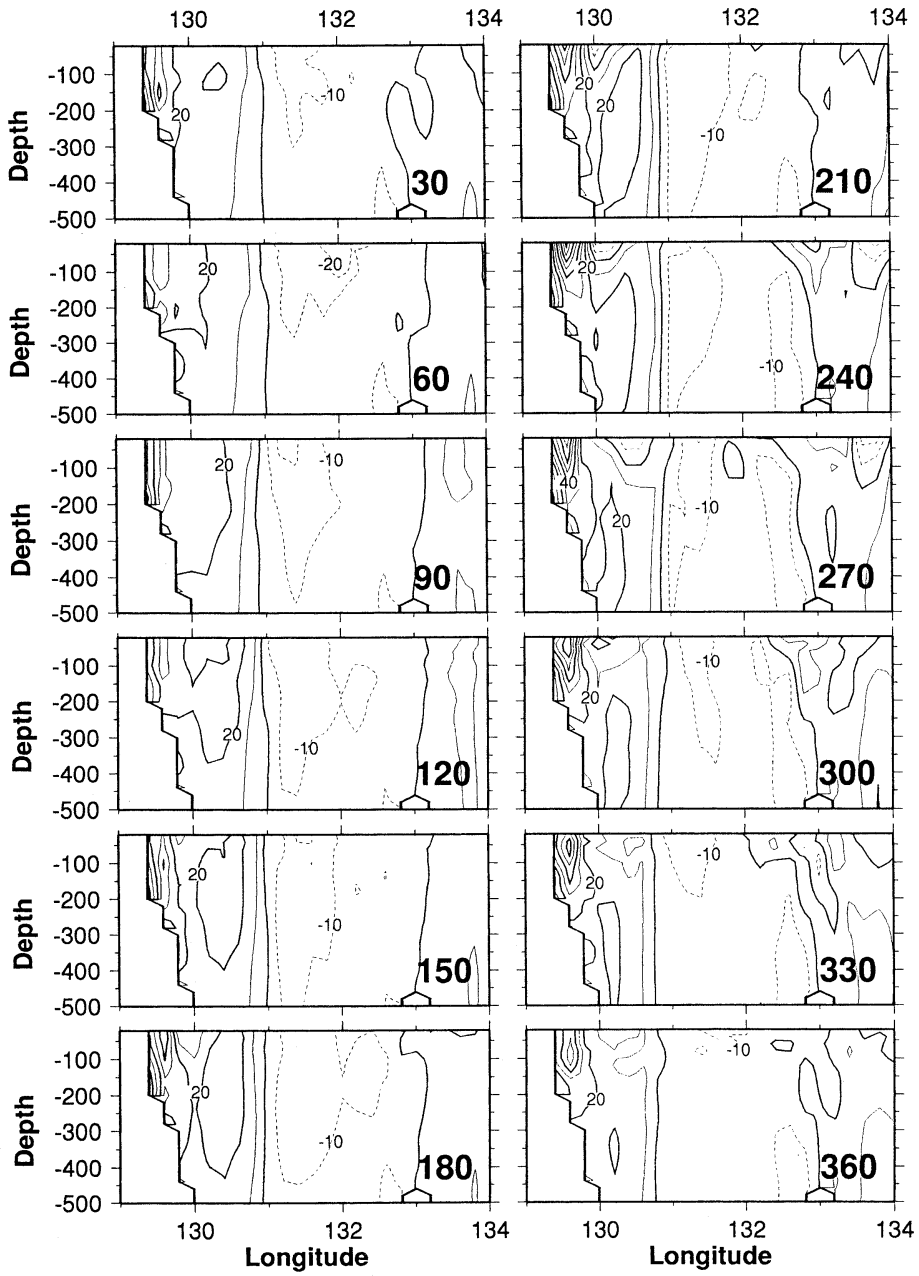

Fig. 7. Vertical sections of v-component along 37° N in climatological run plotted at 30 day intervals. Contour interval is 10cm/s and negative contours are dashed.

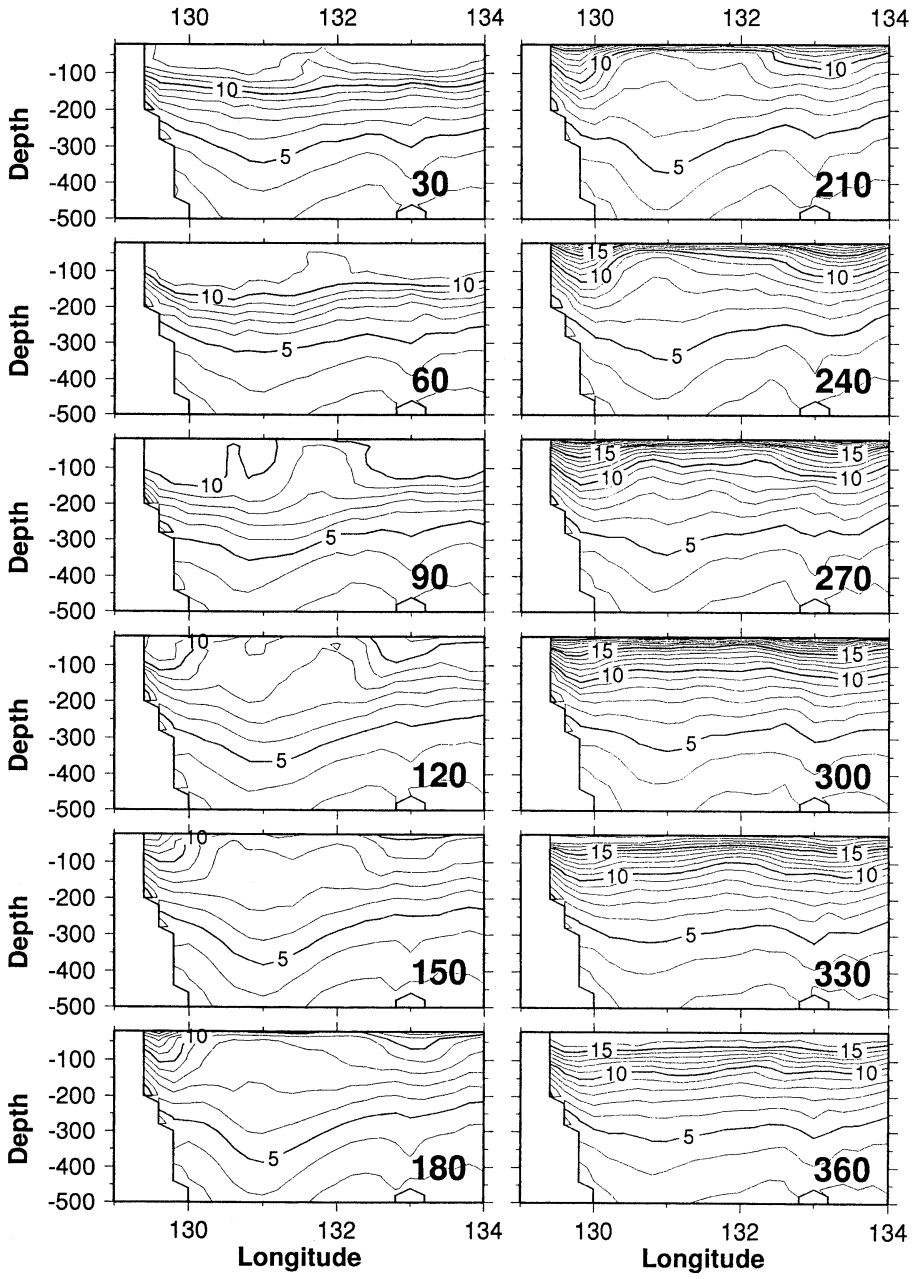

Fig. 8. Vertical sections of temperature along 37°N in climatological run plotted at 30 day intervals. Contour interval is 1℃.

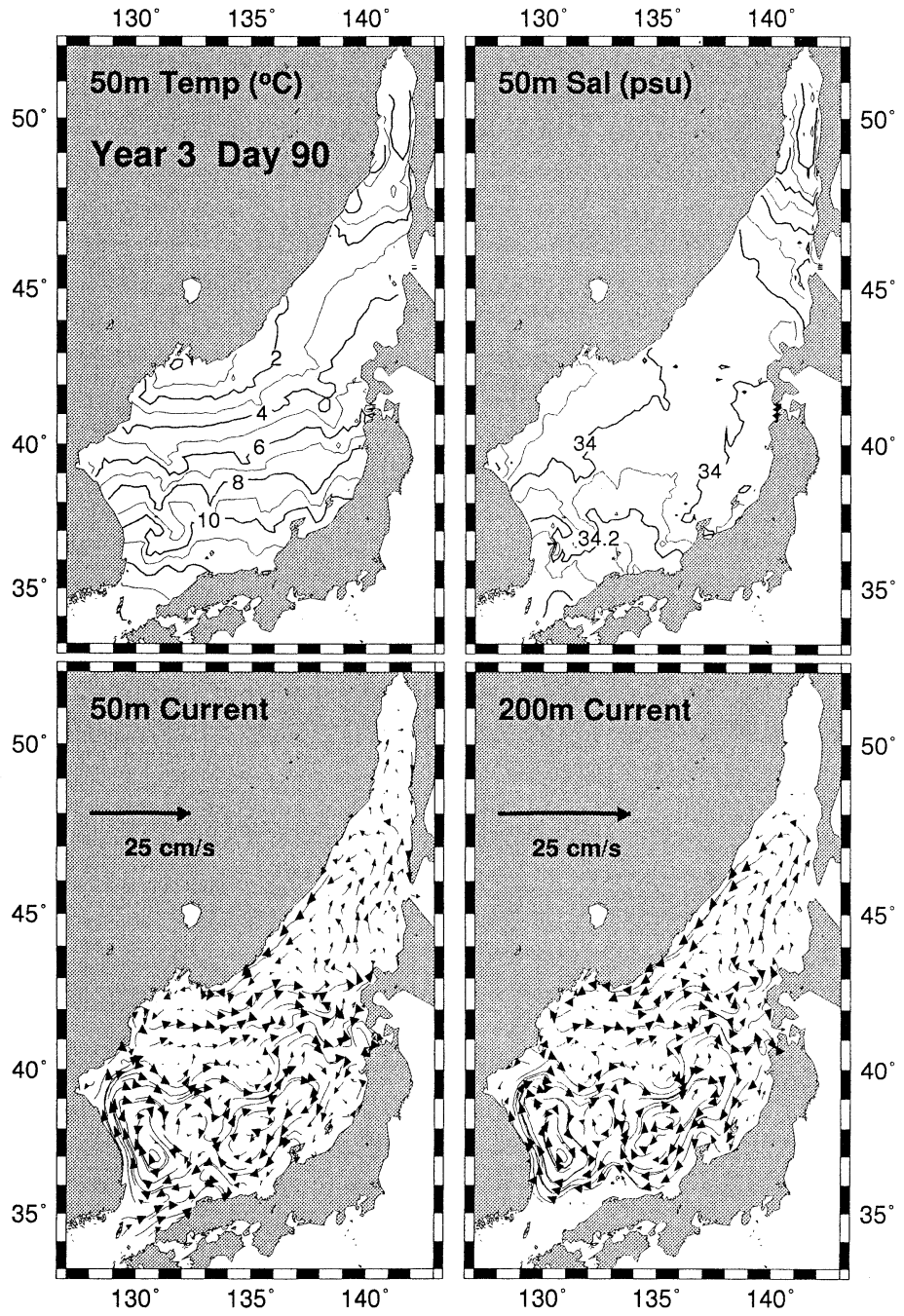

Fig. 9. Temprerature and salinity at 50m, and streak plots at 50m and 200m for a winter day in the climatological run. The EKWC intrudes too far to the north and the NKCC is nearly absent.

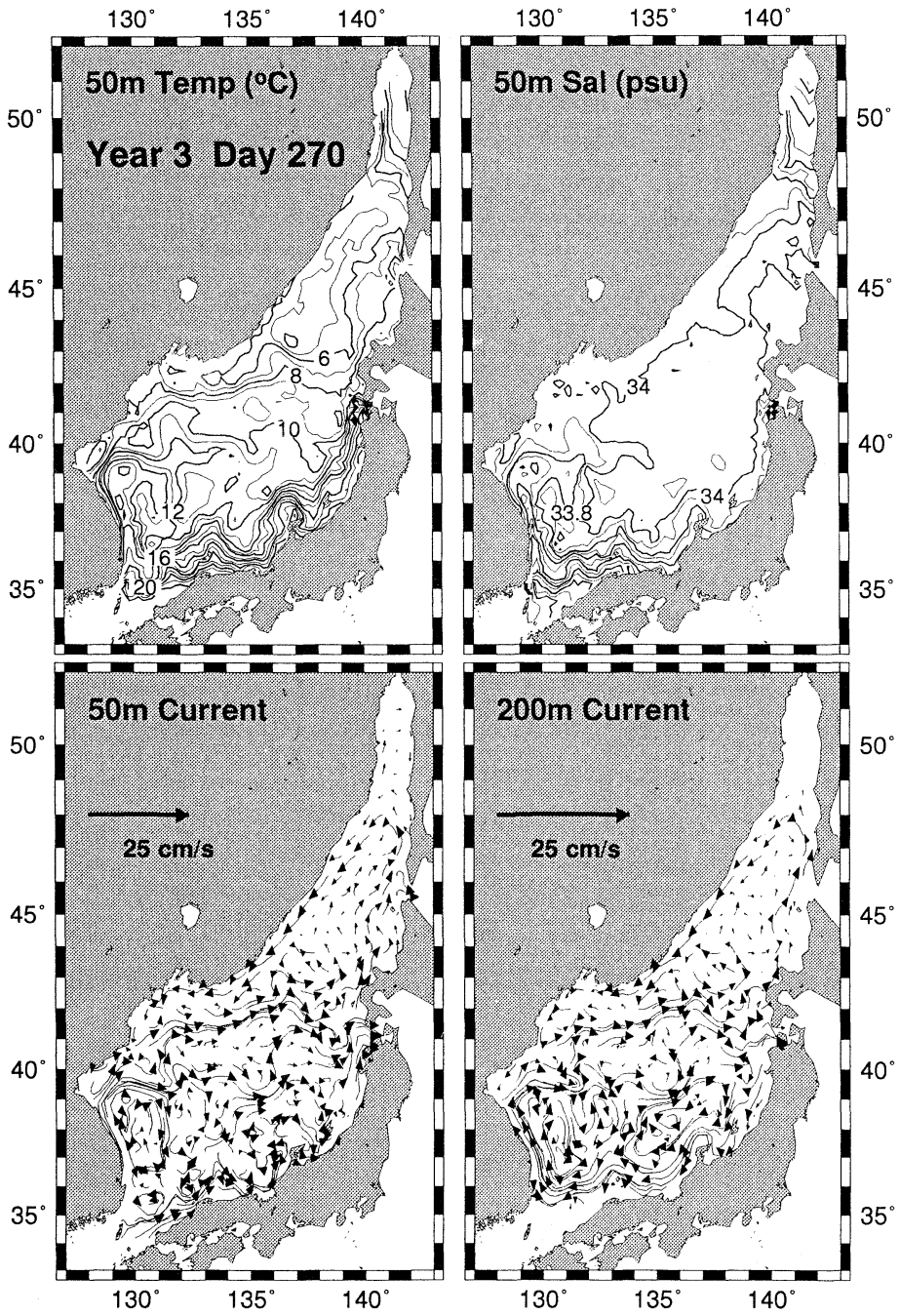

Fig. 10. Temperature and salinity at 50m, and streak plots at 50m and 200m for a summer day in the climatological run. Note the presence of warm, less saline water along the Japanese coast.

northerly latitude than indicated by observations. One possible cause is the weak wind forcing inherent in climatological forcing, as suggested by the synoptic runs described next. The EKWC continues to the east along the Polar Front.

Another interesting thing to note is the appearance of a counter-undercurrent at depths of 100–200 m underneath the eastward flowing current along the Japanese coast, which has also been observed in other model simulation (KIM and YOON, 1994; YOON, 1991; SEUNG and KIM, 1993).

Figure 9 and 10 show temperature, salinity, and current at 50m and current at 200m depth for winter and summer conditions. During the first 3-4 months of the year temperature and salinity at 50m resembles the distribution at the surface indicating strong influence from the surface either by advection (sinking) or by diffusion or both. After this period the pattern of temperature and salinity becomes complicated and resembles more closely a circulation pattern. This suggests that the distribution of temperature and salinity is controlled by horizontal advection. It is interesting to note that the flow that branches off from the separated EKWC to the south and around the center of the UWE is also seen in the temperature and salinity distributions at day 90 as an intrusion of cold and less saline waters.

The circulation at 200m depth is not much different from the 50m circulation pattern. Like in the upper layer, there is a northward-flowing boundary current along the Korean coast, it separates from the coast and flow to the east. One major difference is the presence of a consistent and strong westward flow along the southern perimeter. This flow joins to the northward flow along the Korean coast thus closing the anticyclonic circulation.

3.2 Synoptic Simulation for 1993

The major difference in this synoptic simulation compared to the climatological one described above is that the EKWC separation is more realistic, at 37–38° N rather than 38–39° N (Fig. 11). This suggests that the separation point depends strongly on the strength of wind forcing applied over the basin. One immediate consequence of the change of the separation latitude is that the shape of UWE is now more nearly circular than in the climatological case.

Figure 12 shows the currents at various depths on day 90. Strong branching of the inflow into the EKWC and JWC can be seen at 50 m depth. The EKWC turns eastward at a latitude of 39° N and branches into two strong streams, one proceeding towards Tsugaru and the other towards Soya Straits. The Liman Current (LC) and the North Korean Cold Current (NKCC) can be clearly seen at 200m depth. These multiple current systems are responsible for the various thermal fronts seen running east-west in thermal imagery. The surprisingly strong barotropic nature of currents in the East Sea can be seen in plots of currents at various depths. Recent observations by TAKEMATSU *et al.* (1994) suggest the existence of strong nearly barotropic currents at depths as large as 3000m in the Japan basin.

The time-longitude plot of sea level along 37° N is similar to the one with climatological wind except the development of high-frequency components (Fig. 13). Quite naturally, this is because the winds used in this simulation contain more high-frequency variability both in time and space than the monthly averaged climatological winds.

In the temperature section along 37° N (not shown), the bulging of isotherms in the upper 200m that leads to the temperature homogenization in the climatological case is weaker. However, the velocity of EKWC shows similar behavior as in the climatological case that the magnitude of the core velocity is over 70cm/s during days 210–270 and a southward flow develops during the same period (not shown).

The strengthening of the EKWC and the appearance of a southward flow just offshore of EKWC and the UWE are closely related. It is possible that the strengthening of the EKWC leads to the development of an anticyclonic recirculation cell just south of the separation point. When the EKWC becomes weak after the peak inflow from the Korea Strait, the anticyclonic vorticity in the recirculation cell might diffuse to a wider area leading to the reappearance of UWE in the south.

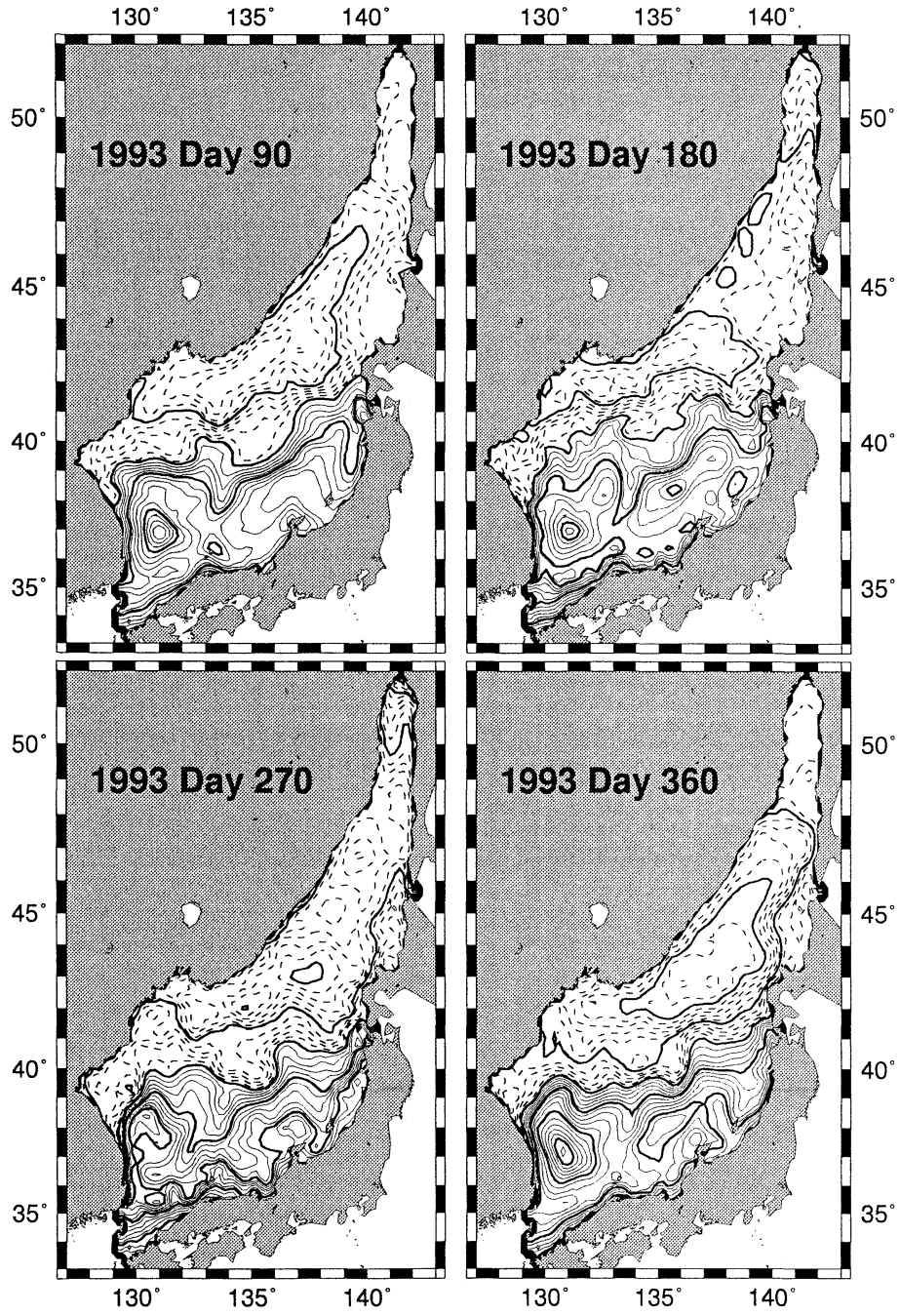

Fig. 11. Seasonal variation of sea level distribution of the synoptic run. Contour interval is 2cm and the negative contours are dashed ; thick lines indicate contours at 10cm intervals.

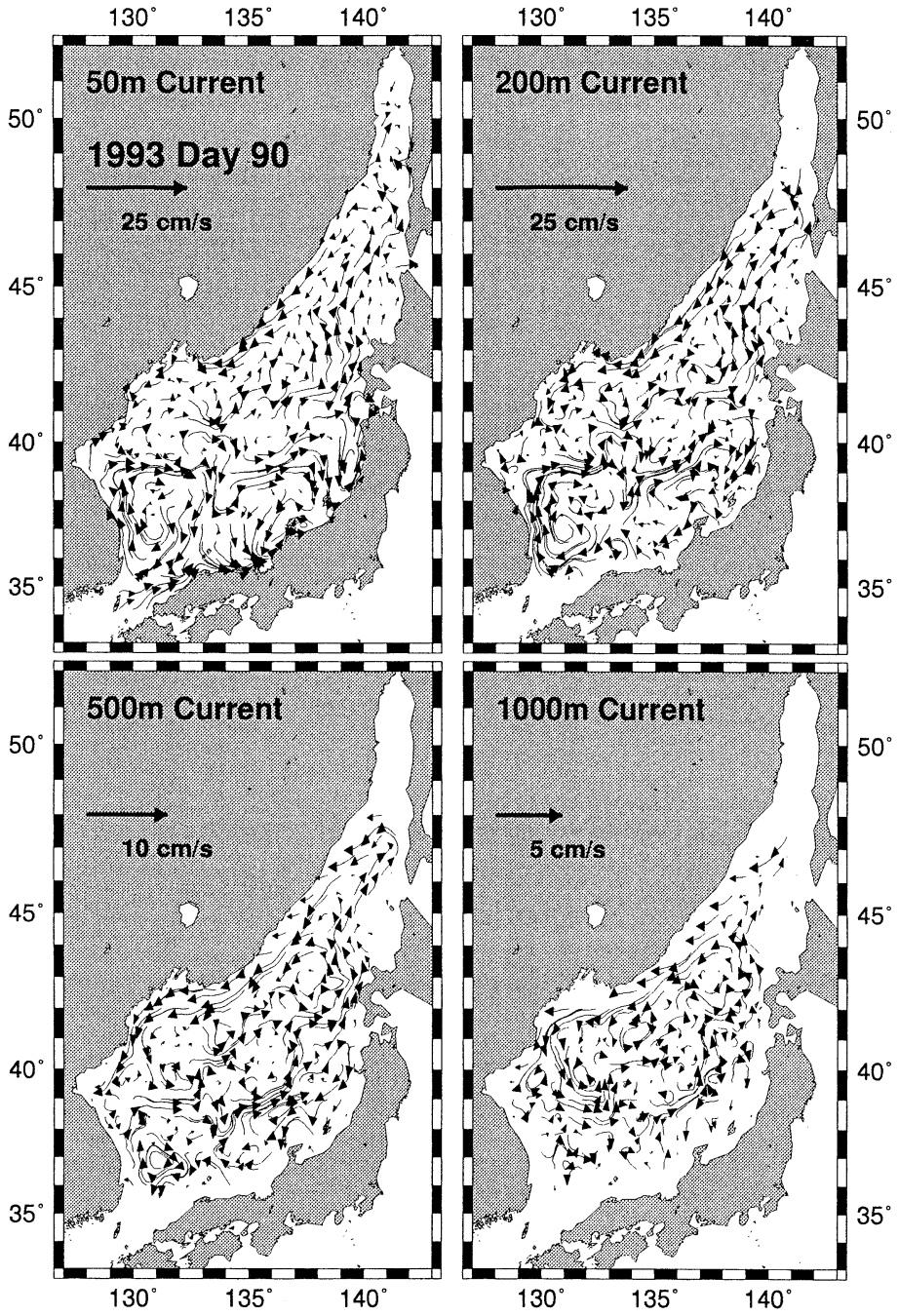

Fig. 12. Streak plots of currents at 50m, 200m, 500m and 1000m depths. Note the difference in scales. Note also the strong barotropic nature of currents, and the strong recirculation at depths below the sill depth at Korea Strait.

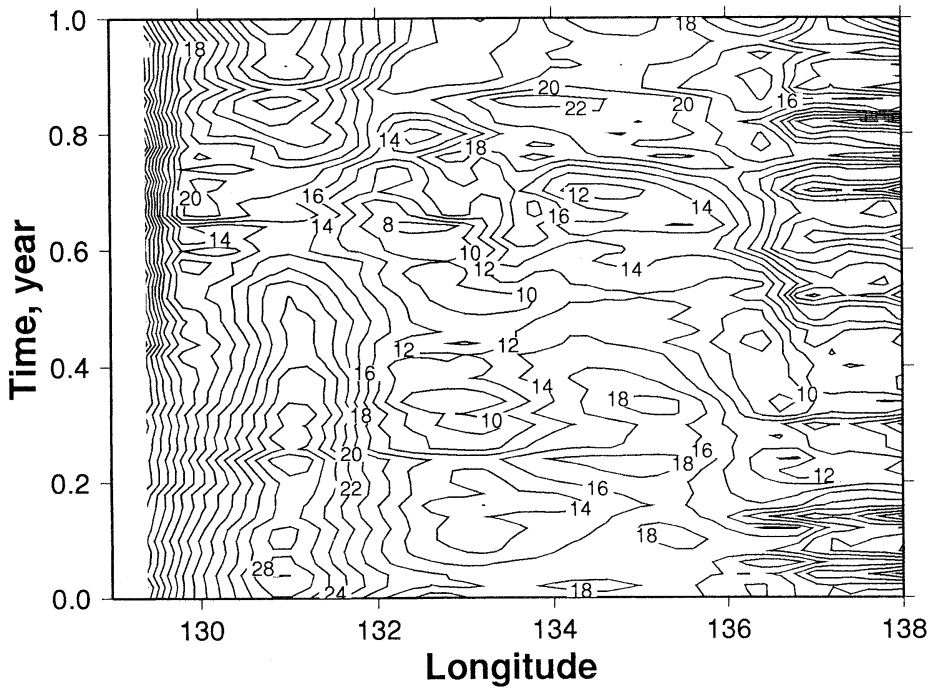

Fig. 13. Time-longitude plot of sea level (in cm) along 37°N of the synoptic run.

3.3 Hindcast

Appropriate weighting of observations and model results are an essential part of any assimilation sheme. While sophisticated schemes such as Kalman filters are ideally suited for this purpose, and take advantage of the known observational and computed model error statistics, they are prohibitively expensive and impractical for a nowcast/forecast system such as this. The simple OI scheme used with a proper choice of the weighting factor can take advantage of both dynamics and observations. Three different weighting factors (10, 20, 30%) were therefore tried.

We chose the drifter buoy tracks of LIE *et al.* (1995) as an independent set of observations to compare and verify our model results. Comparison of the TOPEX altimetry data with drifter tracks shows a remarkable agreement between the two. In particular, an anticyclonic eddy in which the two drifters were trapped for a while is also clearly seen in TOPEX altimetry (Fig. 14). This eddy is a robust feature in the altimetry data and therefore we focused on an accurate representation of this eddy in the nowcast.

Figure 15 shows results at day 180 with different weighting factors. With 10%, the anticyclonic eddy shows up, but the size and location are not exactly the same as in TOPEX data. With 20%, there is not much difference from 10% but the eddy manifests itself more clearly. Increasing the weighting factor to 30%, however, does not help, since the eddy is now joined to the another anticyclonic circulation from the south losing its identity as an isolated eddy. Also, the sea level field becomes more plagued by high-frequency components.

As a check on the assimilation method, the sea level from the 0% assimilation run was subtracted from results of assimilation runs (Fig. 16). The resulting plot shows that the anticyclonic eddy detected by TOPEX is clearly seen. But the strength of the eddy is weaker than the TOPEX-detected signal which has about 8 cm rise above from the surroundings. Nonetheless, it is clear that the method works.

Of the three assimilation experiments, one with 20% weighting appears to best generate

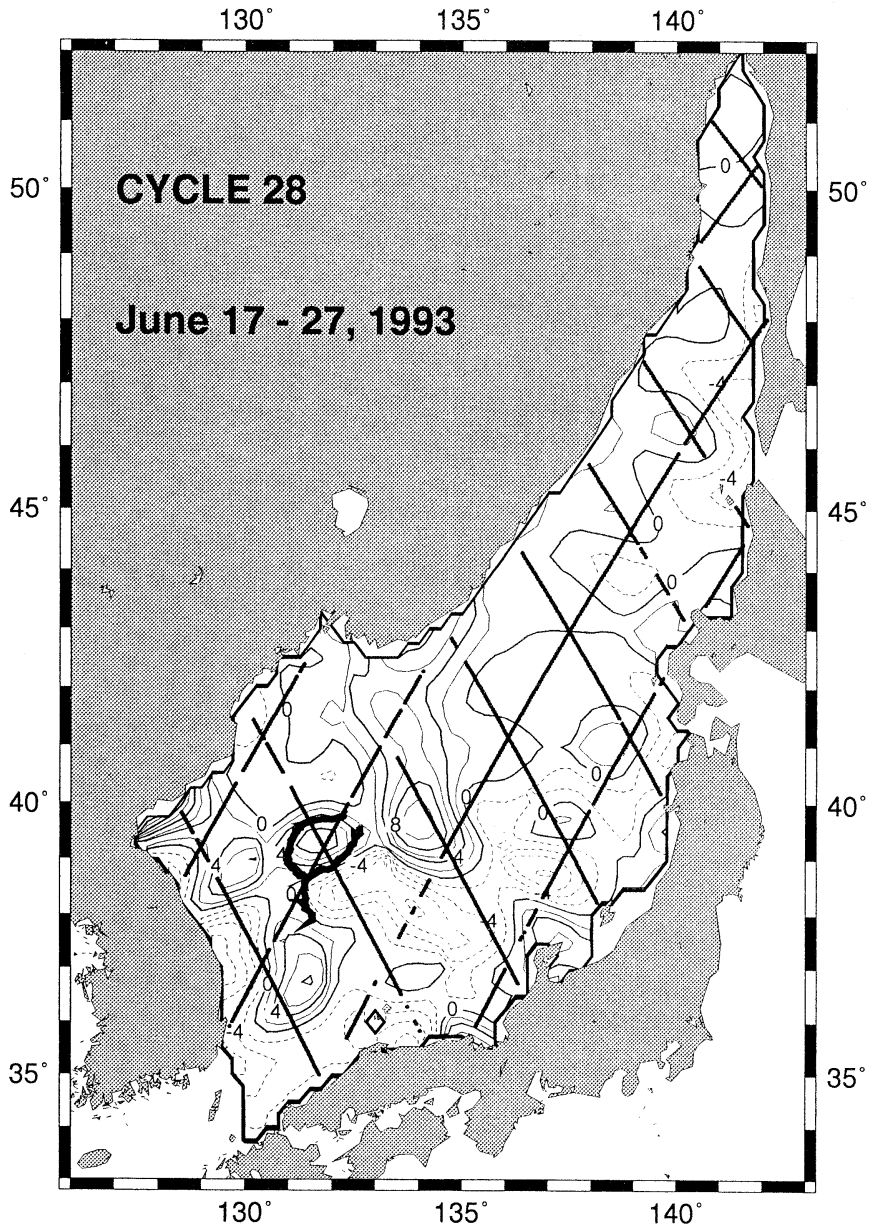

Fig. 14. Optimally interpolated sea level anomaly of TOPEX Cycle 28 (June 17–27, 1993) and two WOCE drifter buoy tracks during the same period. Contour interval is 2 cm and negative values are dashed. Heavy lines indicate satellite tracks.

anticyclonic eddy. To see if different winds affect the result we also ran a hindcast with winds derived from synoptic charts of Japan Meteorological Agency by NA *et al.* (1992). The weighting factor is 20% and the run is started from the climatological run as before. Figure. 17 shows comparison with FNMOC wind case. While this result shows stronger anticylonic eddy than with FNMOC wind, the defferences between the two are small.

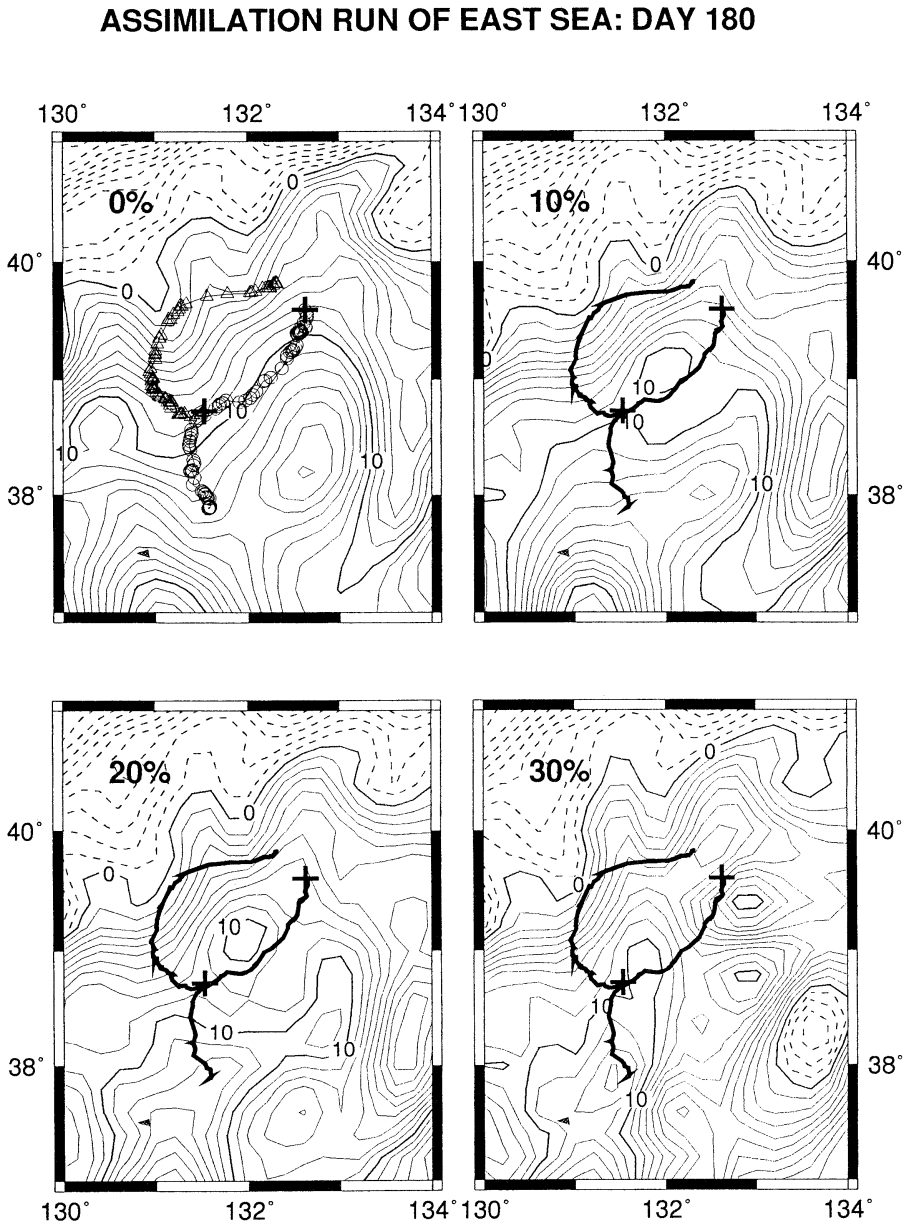

Fig. 15. Sea level distributions at day 180 from assimilation runs with various weighting factors. Contour interval is 1 cm and negative values are dashed. Plusses indicate the beginning of the drifter tracks.

4. Discussion and conclusions

The climatological simulation and the synoptic run appear to successfully reproduce many of the well-known circulation features in the ES. They also show an anticyclonic eddy, the UWE, south of Ulleung Island over the deep Ulleung basin almost all year round in the sea level signal. From these model simulations, there appears to be a close connection between the inflow from the Korea Strait, the EKWC and the UWE. The topography of the Ulleung basin also determines the location, and the

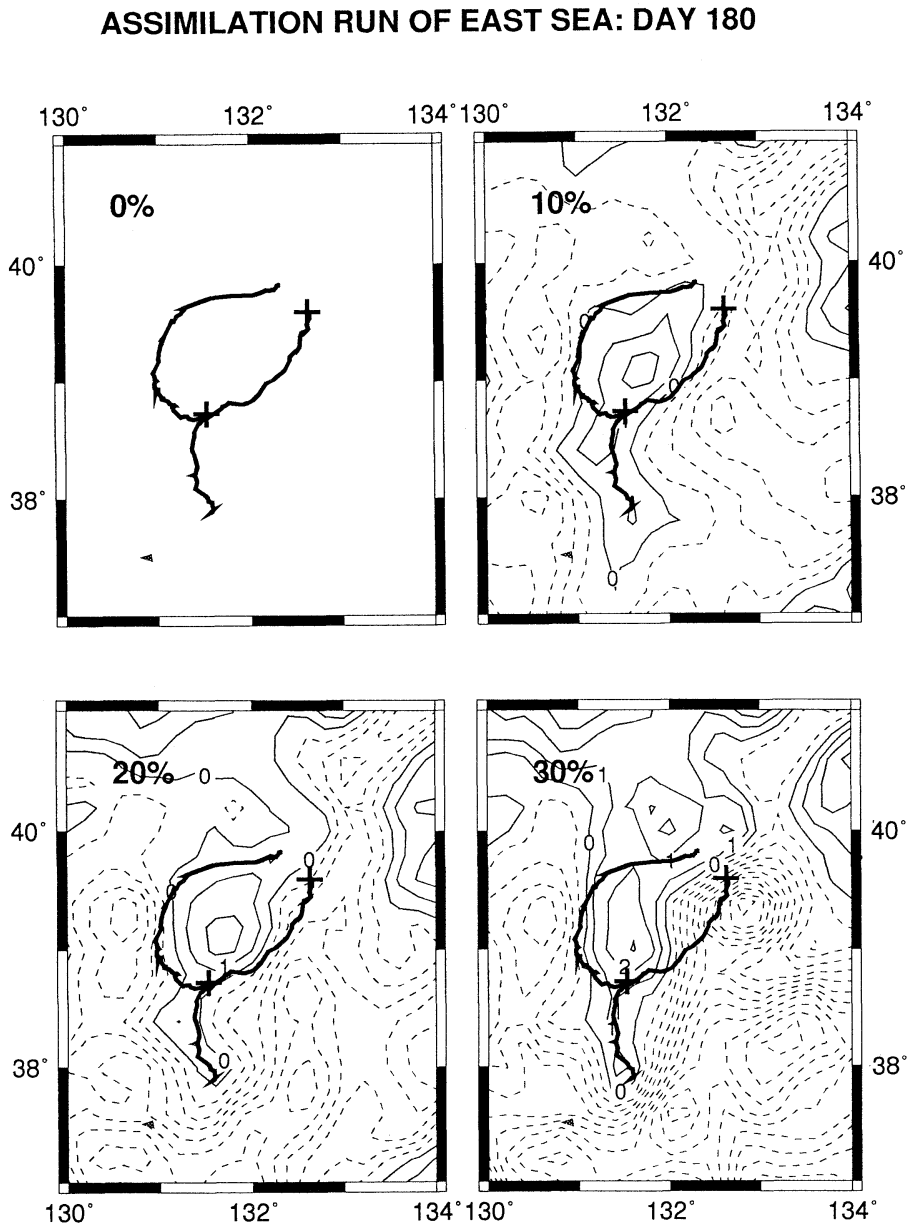

Fig. 16. Difference in sea level between runs with various weighting factors and without indicate the beginning of the drifter tracks.

formation and decay of the UWE.

A faithful simulation of the circulation in any basin depends on many factors. Of these, an accurate prescription of model forcing is of utmost importance. In the ES circulation, wind stress, surface heat/salt fluxes, inflow through the Korea Straits are all important. In this study, only the wind data is synoptic, but the other two forcing came from a climatological source (surface heat/salt fluxes) and a short term observation (inflow condition). Using observed sea surface temperature fields or

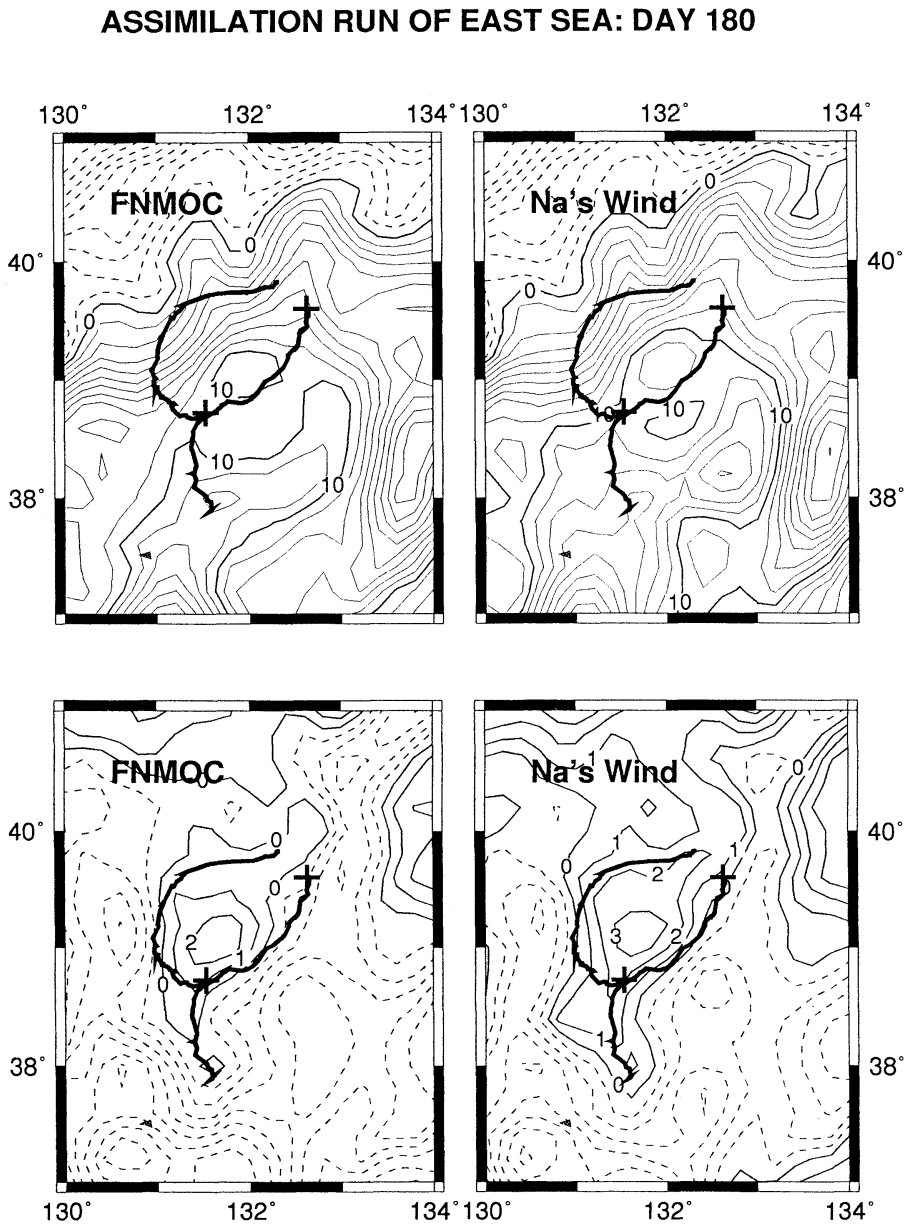

Fig. 17. Comparison of results with Na's and FNMOC winds. The upper panel shows sea level distribution and the lower panel is the difference from 0% weighting. Contour interval is 1 cm and negative values are dashed. Plusses the beginning of the drifter tracks.

thermohaline fluxes from Numerical Weather Prediction (NWP) products would improve the results. The inflow prescription is however problematic. Without long term observations in the Korea/Tsushima Straits, it is nearly impossible to prescribe correct inflow conditions.

Improvement can also be made in the assimilation method. In this study, we used one relationship for the conversion of altimetry anomaly into vertical temperature anomaly profile for the whole ES region. It might therefore be desirable to divide the ES at least into

two regions; northern half and southern half of Polar Front because they have different TS characteristics; the southern warm water has a salinity maximum layer due to the inflow of warm and saline Tsushima Current while the northern cold water does not have this feature. However, the results depend very much on the data density. Since the data are concentrated in regions south of the Polar Front, the result will be biased towards this relatively data-rich region.

Another significant problem we do not have a solution to, is how to derive the true reference state for the assimilation of temperature anomalies. This is simply because we can derive only the SSH anomalies from altimetry. It is not yet possible to separate the predominant geoid in altimetry accurately enough, and a global along-track mean must be subtracted out from each along-track observation. This means that the reference state of the altimetric SSH anomalies remains unknown. In this study, we used monthly mean temperatures from the model run with no assimilation but, this may not represent the true monthly mean values. It is possible to improve results somewhat through iteration by updating the reference temperature using the result from the previous run.

The only other routine observation being made is by the IR sensors on NOAA polar-orbiting operational satellites. MCSSTs form the most prolific data set available. Normally, MCSST only describes the temperature of the mixed layer and is therefore not generally very useful, especially during summer, when the mixed layer is shallow. However, for the ES, where the variability is principally in the upper 200 m, of which the mixed layer is a significant fraction, assimilation of MCSST in combination with altimetric data is perhaps the best strategy for a nowcast/forecast system. MCSSTs are being assimilated routinely in an operational nowcast/forecast system in the Mediterranean (Horton et al., 1996). Our future work will involve extension of the now cast/forecast system in the ES to include MCSSTs. The boundary conditions imposed at the inflow and outflow ports are another crucial detail that need revisiting and refinement.

Acknowledgments.

LHK acknowledges with great pleasure the support by NAVO under contract IPA-OCG 0800 B. Support was also provided to LHK by the NOMP program of the Office of Naval Research under contract N 00014-92 C-6011, administered by Tom Curtin, and the Coastal Sciences Section of the Office of Naval Research under contract N00014-92-J-1766 administered by Thomas Kinder.

References

BLUMBERG, A. F. and G. L. MELLOR (1987): A description of a three-dimensional coastal ocean circulation model. *In* Three-Dimensional Coastal Ocean Models, (Heaps, N. ed.) American Geophysical Union, 1-16.

CHOI, J. -K., L. H. KANTHA, R. R. LEBEN and C. HORTON (1996): A nowcast/forecast experiment in the Gulf of Mexico. To be submitted to J. Atmos. Ocean. Technology.

HELLERMAN, S. and M. ROSENSTEIN (1983): Normal monthly wind stress over the world ocean with error estimaes. J. Phys. Oceanogr., **13**, 1093-1103.

HORTON, C., M. CLIFFORD, J. SCHMITZ and L. KANTHA (1996): A real-time nowcast/forecast system for the Mediterranean Sea. Submitted to Dyn. Atmos. Oceans.

INOUE, N., T. MIITA and S. TAWARA (1985): Tsushima Strait II: physics. *In* Coastal Oceanography of Japanese Islands, (KUNISHI H. *et al.*, ed) Tokyo Univ. Press, 914-933.

ISOBE, A., S. TAWARA, A. KANEKO and M. KAWANO (1994): Seasonal variability in the Tsushima Warm Current, Tsushima-Korea Strait. Continental Shelf Res., **14**, 23-35.

ISODA, Y. and S. SAITOH (1993): The northward intruding eddy along the east coast of Korea. J. Oceanogr., **49**, 443-458.

KANTHA, L. H. and C. A. CLAYSON (1994): An improved mixed laver model for geophysical applications. J. Geophys. Res., **99**, 22535-25266.

KANTHA, L. H. and S. PIACSEK (1993): Ocean Modeling. *In* Computer Science Education Project Electronic Book, Department of Energy, pp. 73.

KANTHA, L. H. and S. PIACSEK (1996): Computational Ocean Modeling. To appear in CRC Handbook of Computer Science and Technology.

KIM, C. (1993): A study on the meso-scale warm eddy in the southwestern part of the East Sea. Res. Rep., BSPN 00187-611-1, KORDI, Korea.

KIM, C. -H., H. -J. LIE and K. -S. CHU (1991): On the intermediate water in the southwestern East Sea (Sea of Japan). *In* Oceanography of Asian Mar-

ginal Seas, (Takano, K. ed.) Elsevier, 129–141.

KIM, C. -H. and J. -H. YOON (1994): A numerical study on the seasonal variation of the Tsushima Warm Current along the coast of Japan. Abstract of Third Workshop of Circulation Research of the East Asian Marginal Seas, November 7–8, Seoul, Korea.

KIM, K. and J. Y. CHUNG (1984): On the salinity–minimum layer and dissoved oxygen – maximum layer in the East Sea (Japan Sea). *In* Ocean Hydrodynamics of the Japan and East China Seas,(Ichiye, T. ed.) Elsevier, 55–65.

LEVITUS, S. (1981): Climatological atlas of the world ocean, NOAA Professional Paper No.13, U. S. Govt. Printing Office, pp. 173.

LIE, H. -J., S.-K. BYUN, I, BANG and C. -H. CHO (1995): Physical structure of eddies in the southwestern East Sea. J. Oceanol. Soc. Korea, **30**, 170–183.

MELLOR, G. L. (1992): User's guide for a three–dimensional, primitive equation, numerical ocean model. Program in Atmospheric and Oceanic Sciences Report, Princeton University, pp. 35.

MORIYASU, S. (1972): The Tsushima Current. *In* Kuroshio, (Stommel, H. and K. Yoshida, ed.) Univ. Tokyo Press, 353–369.

NA, J. Y., J. W. SEO and S. K. HAN (1992): Monthly-mean sea surface winds over the adjacent seas of the Korean Peninsula. J. Oceanol. Soc. Korea, **27**, 1–10.

SEKINE, Y. (1988) On the seasonal variation in in and out–flow volume transport of the Japan Sea. Prog. Oceanogr., **21**, 269–279.

SENJIU, T. and H. SUDO (1993): Water characteristics and circulation of the upper portion of the Japan Sea proper Water. J. Mar. System, **4**, 349–362.

SEUNG, Y. -H. and K. KIM (1993): A numerical model of the East Sea Circulation. J. Oceanol. Soc. Korea, **28**, 292–304.

SHIN, H. -R., S. -K. BYUN, C. KIM, S. HWANG and C. -W. SHIN (1995): The characteristics of the structure of warm eddy observed to the northwest of Ullungdo in 1992. J. Oceanol. Soc. Korea, **30**, 39–56.

TAKEMATSU, M., A. G. OSTROVSKII and T. KITAMURA (1994): Current feature in the Japan Sea's proper water. Abstract of Third Workshop of Circulation Research of the East Asian Marginal Seas, November 7–8, Seoul, Korea, 1994.

YOON, J. -H. (1991): The branching of the Tsushima Current. Report, Res. Inst. Appl. Mech., Kyushu Univer., **38** (108), 1–21.

Received December 12, 1995
Accepted March 22, 1996